Opt Quant Electron (2007) 39:677–686
DOI 10.1007/s11082-007-9118-0

Photonic crystal-based dual-band demultiplexers on silicon materials

Lung-Wei Chung · San-Liang Lee

Received: 31 March 2005 / Accepted: 28 August 2007 / Published online: 25 September 2007

Abstract This investigation presents a novel design of dual-band demultiplexers based on a periodic hexagonal lattice of holes or rods on silicon materials. The demultiplexing function can be applied by coupling between two defect waveguides at one wavelength with no coupling then at another wavelength. Appropriately choosing the radius and number of separated rows yields a broad bandwidth for one range of wavelengths. Two designs that use rods or holes to generate photonic crystals are realized. An analysis based on finite-difference time-domain (FDTD) and plane wave expansion (PWE) methods demonstrates that a 1.3/1.55 μm dual-band wavelength demultiplexer can have a very low insertion loss and high isolation ratio.

Keywords Photonic crystals · Wavelength demultiplexer · Directional coupler · Photonic bandgap · Line defect waveguide

1 Introduction

Dual-band wavelength demultiplexers (DBWDs) are commonly used in bi-directional and/or access communication networks. For instance, 1.3/1.55 μm duplex devices are in high demand for use in fiber-to-the-home (FTTH) and other bidirectional transmission systems. Discrete fiber-based components are frequently used to build DBWDs, and photonic integrated DBWDs are very attractive because of their low cost and compactness. Photonic crystals (PhCs) have very promising material structures for fabricating photonic integrated DBWDs because they are compact and provide unique mechanisms for controlling optical waves (Yablonovitch 1987).

Photonic crystal waveguides (PCWs) that are generated from line defects in a PhC structure can very effectively confine and control the light propagation. They exhibit less

L.-W. Chung (✉) · S.-L. Lee
Department of Electronic Engineering, National Taiwan University of Science and Technology, 43 keelung Road, Sec. 4, Taipei, 106 Taiwan, ROC
e-mail: D9102304@mail.ntust.edu.tw

radiation loss from the sharp bends than conventional waveguides (Vlasov and McNab 2004). Studies have established both experimentally (McNab et al. 2003) and theoretically (Tanabe et al. 2007) that various optical characteristics PCWs differ from those of conventional waveguides because of photonic bandgap (PBG) effects. PhC-based components with high transmission bandwidths have been mentioned (Chutinan et al. 2002). Wavelength demultiplexers and channel drop filters (Imelda et al. 2002) have been developed by utilizing various combinations of point defect cavities or bandpass resonators (Costa et al. 2003) and by setting a suitable radius for the defects and suitable positions along the PCWs (Koshiba 2001). These PhC-based devices can be formed from either rods or air holes (Sharkawy et al. 2002).

This investigation adopts the directional-coupler (DC) type structure that comprises two parallel line-defect waveguides to realize a DBWD device (Martinez et al. 2003). The switching performance of the coupled waveguide is generally sensitive to the wavelength. A high isolation ratio (or crosstalk suppression) and low insertion loss are critical parameters that govern DBWD devices. Furthermore, a broad optical bandwidth is required to support the wavelength fluctuation of signal sources for some system applications such as wavelength-division-multiplexing (WDM) networks. In particular, the 1.3-μm band for passive optical networks(PONs) must be wide enough to tolerate the relative large wavelength drift of coolerless FP lasers.

A novel design for parallel line-defect waveguides is proposed. It involves differentiating the coupling and decoupling mechanisms at various wavelength bands. The characteristics of the device are analyzed using the plane-wave expansion (PWE) method developed by an MIT group (Johnson and Joannopoulos 2001). The performance is confirmed by the high isolation ratio and broad bandwidth at the bar state by applying the finite-difference time domain (FDTD) method.

2 Directional-coupler demultiplexer

Figure 1 depicts the device structure of the PhC-based DBWD with two parallel line-defect waveguides. Areas 1 and 2 refer to the coupling and access regions, respectively. Port 1 is the input port and Ports 2 and 3 are the two output ports. This work presents two designs for DBWD. The first design of the PhC structure involves rods. The second design involves a periodic arrangement of air holes. The parameters Λ and r represent the lattice constant and radius of the photonic crystals, respectively. The holes or rods in the coupling region between the line-defect waveguides have various radii, r_c. L_c represents the coupling length associated with the coupling region. Although silicon and air are used to fabricate the PhC, the results can be extended to other materials by only slightly modifications to the dimensions of the device. The DBWD is treated as a two-dimensional (2D) structure in the numerical calculation to simplify the performance analysis: the heights of both rods and holes are assumed to be infinite. This approach reflects the characteristics of the device and enables the performance to be optimized.

If the line-defect structure is designed to support only two eigenmodes, then the field evolves along the structure as the superposition of these two modes, which are presented as two k-values at the same frequency (ω), for the two $\omega(k)$ curves within the photonic bandgap (Boscolo et al. 2002). When light is incident upon one of the two waveguides, both modes are excited. This condition is typical of the design of a DC-type device. The light is coupled back and forth between the waveguides; the beat length expressed as $L = 2L_c = 2\pi/(k_e - k_o)$, where k_e and k_o are the propagation constants of the even and odd modes, respectively.

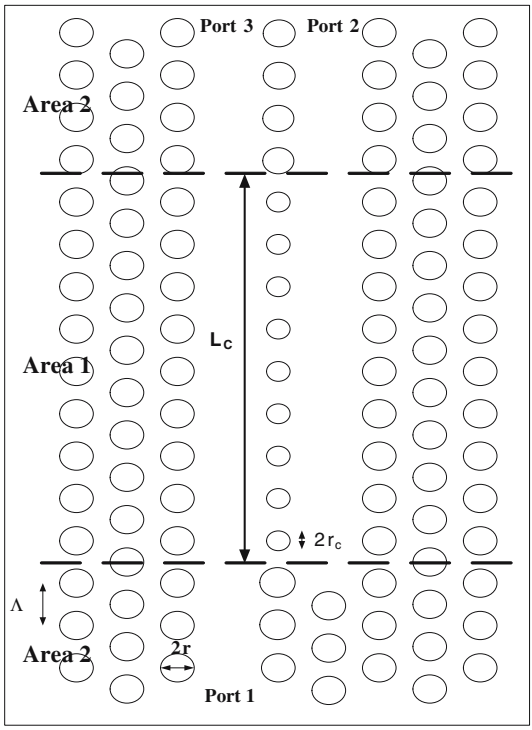

Fig. 1 Illustration of 2D PhC structure. White circles represent rods or air holes

Clearly, the beat length depends on the wavelength at the equation. A DBWD can be realized by selecting a coupler length that directs the two input wavelengths toward different output ports.

The parallel line-defect waveguides enable coupling at one wavelength and decoupling at another. This is a unique characteristic of PhC-based structures when parallel waveguides are separated by an odd number of rows. In such a case, the beat length (L) has a singularity at some wavelength. However, L is a smooth function of wavelength when the waveguides are separated by an even number of rows. The beat length exhibits a singularity when the dispersion curves of the even and odd modes intersect. Accordingly, the two modes are degenerate at the crossover wavelength and light is decoupled between the waveguides.

The coupling and decoupling characteristics of parallel line-defect waveguides were employed in designing wavelength demultiplexers (Chien et al. 2004). In the decoupling state, the field can propagate along a waveguide without coupling. The beat length increases exponentially with the gap between the waveguides, so the parallel waveguides are typically separated by only one row of photonic crystals. Under such conditions, the coupling state will depend strongly on the fluctuation in the coupling length; a high isolation ratio is hard to obtain in both wavelength bands. Adding a ring resonator improves the performance (Chien et al. 2004). Enlarging the separation region to comprise three or more rows of PhCs enables the resultant photonic bandgap to prohibit light from coupling between the waveguides. In such a case, the dispersion curves of even and odd modes completely overlap. Hence, achieving both a good isolation ratio and a low insertion loss is relatively difficult. This study proposes an appropriate radius and number of rows that separate the waveguides and provide a large bandwidth in the bar state with strong crosstalk suppression.

3 Structure design

PhC-based devices on silicon material with low cost and ease of fabrication were designed. The PhC must provide a broad range of PBG to cover two wavelength windows. The PhC structure is formed as a hexagonal lattice of holes or rods, whose PBG is determined by the ratio of the radius to the lattice constant. For a DBWD, light of either wavelength is confined effectively in the line-defect waveguides. The PhC structure is designed to couple the light between the two defect waveguides at one wavelength but to decouple the light at another wavelength in the bar state. The new PhC coupler uses rods and holes whose radii are a function of the row. Such a DBWD design provides a large bandwidth and strong isolation with a simple structure.

The radius of the separate rows is selected to provide a photonic bandgap in the decoupled state and a transparent region in the coupled state. Accordingly, the wavelength of the coupled state is outside the photonic bandgap. Such a design enables more separation rows to be used.

3.1 Silicon rods

The initially designed DBWD is made of a hexagonal PhC of rods (dielectric constant $\varepsilon = 12$) surrounded by air. The radius of the rods in all of the regions, except for the separation region is $r = 0.2\,\Lambda$ ($\Lambda = 0.56\,\mu\text{m}$). When the PWE method is used, the structure has a PBG in transverse magnetic modes (TM polarization) that ranges from 0.263 to 0.449 times the normalized frequency. Two rows of rods are removed from the periodic structure to generate line-defect waveguides. The previous design (Chien et al. 2004) employs rods of the same size across the PhC structure, such that $r_c = r$. Figure 2 depicts an point of intersection between the dispersion curves of the even and odd modes. (e1, e2) and (o1, o2) represent the numbers of even and odd modes. The symmetric mode patterns are confirmed by following the PWE method to determine the modes e1 and o1 in the low-frequency band (f_b), and e2 and o2 in the high-frequency band (f_a). The normalized frequencies $f_a = 0.431$ and $f_b = 0.361$ are considered as useful examples for designing 1.3/1.55-μm DBWD. The splitting of the two curves at f_b and the intersection at f_a realizes coupling at f_b and decoupling at f_a. Such a dual-band demultiplexer has been successfully analyzed (Chien et al. 2004).

As stated above, the decoupling state is associated with a large bandwidth since the line-defect waveguide is formed from photonic crystals with a broad PBG. The light propagates straight forward with a very weak coupling to the adjacent waveguide. However, the coupling state is sensitive to the wavelength. Hence, the rod-based DBWD has a broad band at a wavelength of 1.3 μm but a narrowband at 1.55 μm. If the separation region is enlarged to incorporate three rows of rods, then the curves of the odd and even modes overlap over a wide range of frequencies, as presented in Fig. 2a. The difference wavevector ($\Delta k = k_o - k_e$) at f_b declines as the number of separation rows increases, causing the coupling length at f_b to increase markedly, as revealed by curve 2 in Fig. 2b. The bandwidth at f_a in curve 1 (the width of the normalized frequency at which the curves of odd and even modes overlap with each other) also increases.

The radius of the rods r_c is reduced to a value at which the separation rows do not form photonic bandgap at f_b. To enlarge the coupling factor at f_b in the case with three separation rows are introduced. Accordingly, the coupling of the parallel line-defect waveguides is very similar to that in PLC-based couplers. Figure 3a indicates the dispersion relationship: the difference between the wavevectors of e1 and o1 at frequency f_b increases as the radius

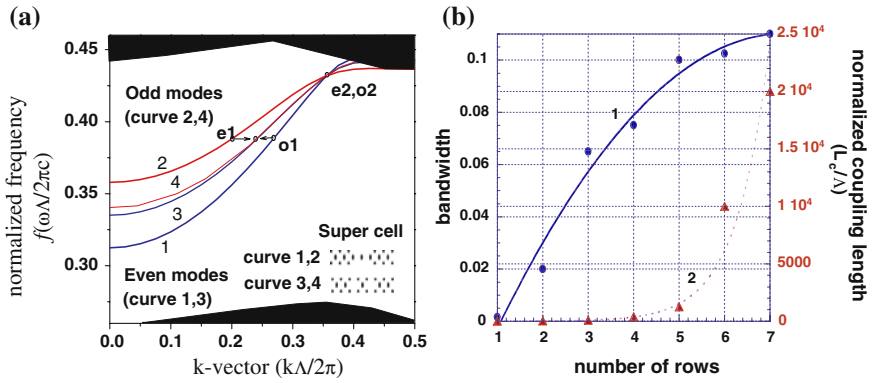

Fig. 2 (**a**) Dispersion curves in the even and odd modes of conventional line defect waveguides, separated with one or three rows of rods; (**b**) difference between wave vectors against number of separating rows. The inset defines the supercells. e1 and o1 represent the even and odd modes at f_a while e2 and o2 are the modes at f_b

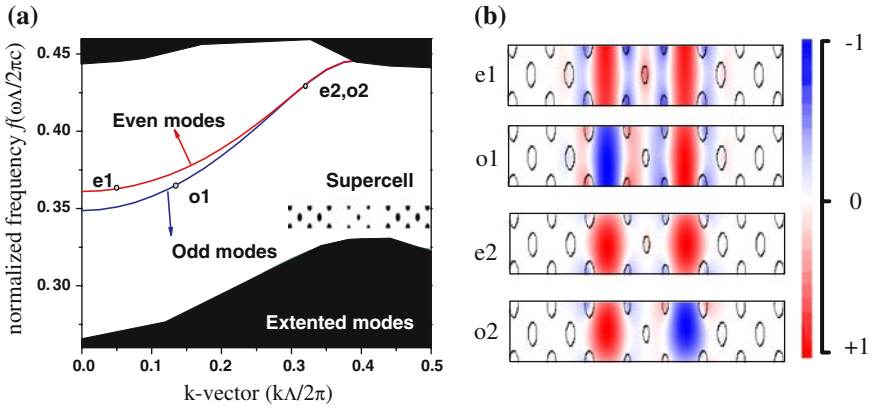

Fig. 3 Dispersion relationship (**a**) and mode fields (**b**) of the new coupler with three separating rows of smaller-radius rods

of the separate rods falls. The mode patterns in Fig. 3b demonstrate the symmetry of the characteristics associated with the defect modes.

Figure 4 compares the coupling lengths associated with the two conventional designs and the new design. Reducing the radius of the separate rods can increase the coupling factor and reduce the coupling length. The results presented in Fig. 4 were obtained by applying the tight-binding approximation (Bayindir et al. 2000). The coupling length is expressed given by

$$L_s = \frac{\pi}{\Delta k} = \frac{\pi}{\cos^{-1}\left(\frac{f_o-\Omega_o}{\alpha_o}\right) - \cos^{-1}\left(\frac{f_e-\Omega_e}{\alpha_e}\right)} \tag{1}$$

if the dispersion curves displayed in Figs. 2 and 3 are approximated by

$$f_i = \Omega_i\,(1 + \alpha_i \cos k_i) \tag{2}$$

where the subscript $i = e$ or o is associated with the even or odd mode, respectively. Therefore, the coupling strength can be controlled by varying the radius r_c of the silicon rods.

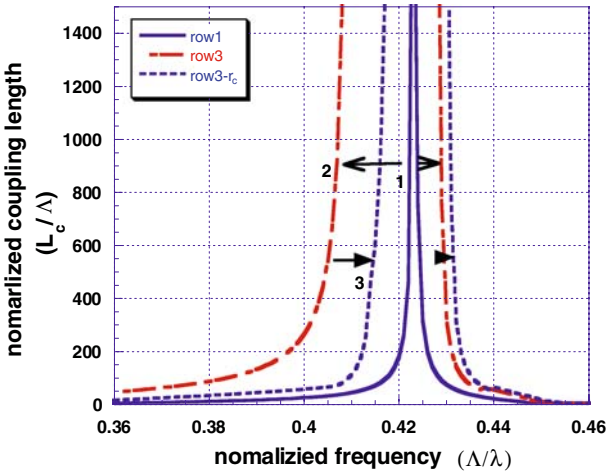

Fig. 4 Normalized coupling length against the normalized frequencies for three coupler designs. Curves 1 and 2 plot conventional designs with one and three separating rows, respectively. Curve 3 is obtained from the design with three separation rows of rods with a small radius

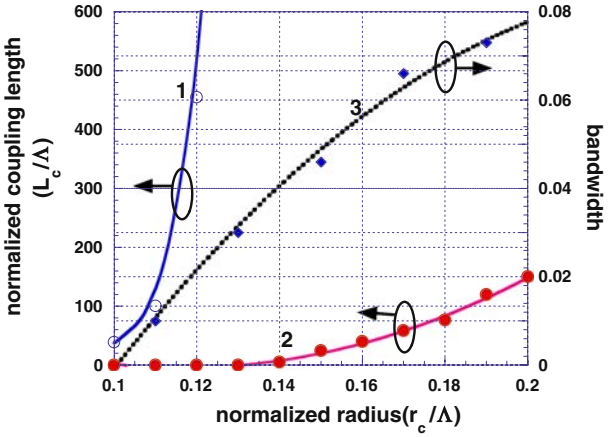

Fig. 5 Normalized coupling length at both frequencies (curves 1, 2) and corresponding bandwidth at frequency f_a (curve 3) versus the radius of the separation rods

Figure 5 plots the normalized coupling length at both bands and the bandwidth at frequency f_a against the radius of the separating rods. The coupling length increases with the radius in both bands. A tradeoff exists between the radius that provides isolation at f_a and the radius that enables coupling at f_b. Given $r_c \geq 0.14\Lambda$ the coupling length is large enough to isolate the two waveguides at f_a. The final choice depends upon the manufacturability and the coupling length at f_b. Additionally, the bandwidth at frequency f_a is sufficiently large when $r_c = 0.14\,\Lambda = 0.112\,\mu\text{m}$. Under such conditions, the light of frequency f_a is transmitted throughout the guide from Port 1 to Port 3, whereas that of frequency f_b is switched entirely to Port 2.

The coupling length is shorter (3.92 μm) than that associated with a PLC-based coupler. The dispersion curves of the e2 and o2 modes nearly overlap at 0.382 to 0.443 times the

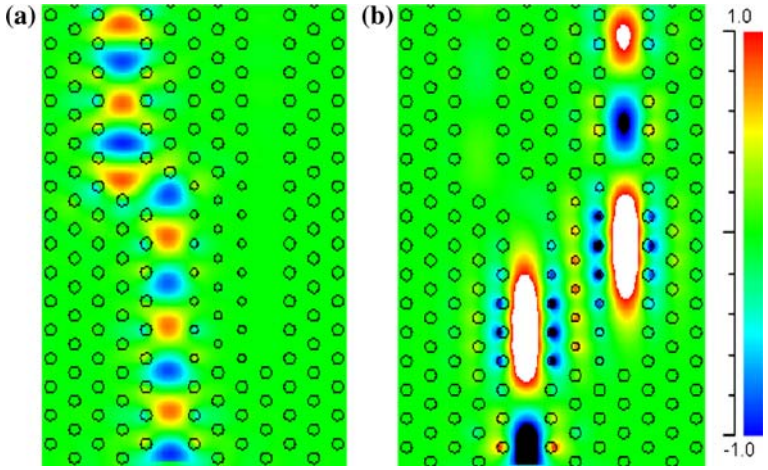

Fig. 6 Field evolution for (**a**) 1.3 µm (f_a) and (**b**) 1.55 µm (f_b) wavelengths along the coupler structure. Five rows of rods are inserted between the output access waveguides to increase the isolation ratio

normalized frequency. In this frequency range, the light propagates without switching to the other waveguide. That is, the beating length at these frequencies is almost infinite at $\Delta k = 0$. The isolation ratio is determined to be approximately 24.5 and 13.2 dB at f_a and f_b, respectively.

Five rows of rods are introduced between the output access waveguides to increase the isolation ratio at f_b. The field evolution displayed in Fig. 6 clearly indicates the demultiplexing function of the PhC waveguides. Figures 6a and b refer to wavelengths of 1.3 and 1.55 µm. The isolation ratio at a wavelength of the 1.55 µm is increased to 16.8 dB without influencing the performance in the bar state at the 1.3 µm band. The calculated insertion loss is under 0.5 dB at both wavelength bands.

3.2 Embedded air holes

PhC-based DBWDs of the second type are made from silicon materials with embedded air holes. The radius of the normal holes is set to $r = 0.4\Lambda$. The PWE method yields a PBG in transverse electric (TE) modes that ranges from 0.245 to 0.393 times the normalized frequency in the ΓK direction. The difference between the refractive index profiles of the holes and the rods cause the dispersion relation of the hole-based PhCs to differ from that of the rod-based PhCs. Hence, a DBWD with a large bandwidth at f_b but a small bandwidth at f_a can be designed. Again, this is a unique characteristic of PhC-based structures.

Let $\Lambda = 0.42$ µm; then, wavelengths of 1.3 and 1.55 µm correspond to $f_a = 0.328$ and $f_b = 0.275$, respectively. The radius r_c of the air holes in the separation region is also varied to modify the coupling strength. When only one separation row is between the two parallel line-defect waveguides, the structure can perform decoupling at f_b but coupling at f_a. Figure 7 plots the normalized coupling length at both frequencies and the bandwidth at frequency f_b versus the normalized radius. For $r_c \geq 0.314\Lambda$, the coupling length is sufficiently large for isolation (decoupling) at frequency f_b and sufficiently small for switching (coupling) at f_a. The light of frequency f_b is transmitted throughout the guide from Port 1 to Port 3, whereas the light at frequency f_a is completely switched to Port 2.

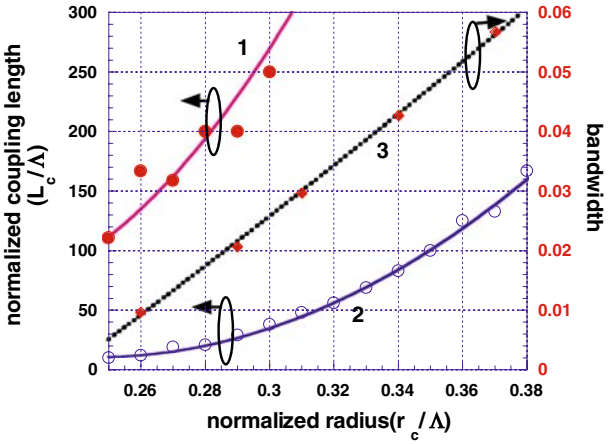

Fig. 7 Normalized coupling length at both frequencies (curves 1, 2) and the corresponding bandwidth at frequency f_a (curve 3) vs. the radius of the separating holes

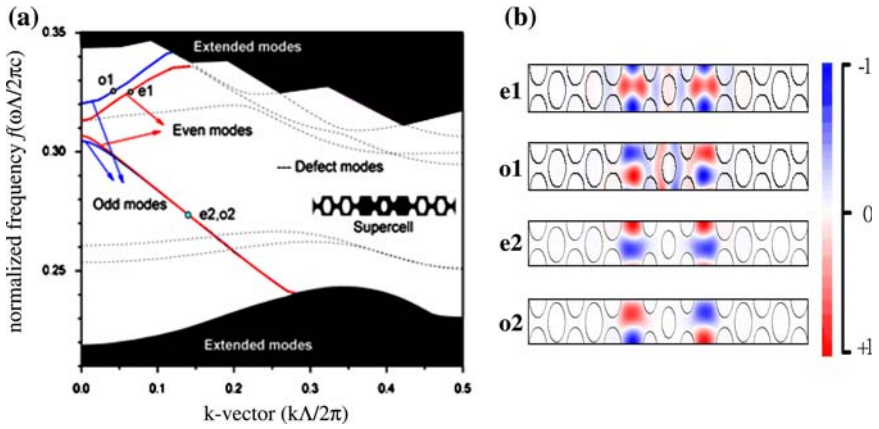

Fig. 8 Dispersion relationship (**a**) and mode fields (**b**) of the air-hole-based couplers with three separating rows of holes with a small radius

The calculated dispersion curves in the modes of structures with one row of holes in the separation region almost overlap from 0.23 and 0.31 times the normalized frequency. When the value exceeds 0.32 in the normalized frequency, the dispersion relationship is split into two curves one for each mode. Accordingly, at $f_a \cong 0.328$, two modes with different wave vectors are excited in the parallel waveguides. The difference between the wave vectors of the modes (e1 and o1) governs the coupling strength. The coupling length is determined according to Eq. 1 to be approximately 9 µm, which exceeds that of the rod-based structure but is much shorter than that of the PLC-based couplers. Restated, the coupling length at these frequencies is infinite and a broadband bar state is determined, as it is using the rod-based DEMUX. The calculated field evolution at wavelengths of 1.55 µm (f_b) and 1.3 µm (f_a) again reveals the de-multiplexing of the structure. An isolation ratio of 7.6 and 23.9 dB can be obtained at wavelengths of 1.3 and 1.55 µm, respectively. The plots of simulated isolation ratio and insertion loss as a function of coupler length demonstrate that the best coupling length is around 9.2 µm which is consistent with the approximation.

Three rows of air holes are made between the waveguides to increase the isolation ratio of light in the bar state. Figures 8a and b plot the dispersion relationship and mode patterns, which are very similar to those in the one-row case. The even and odd modes almost overlap each other over the range between 0.23 and 0.29 in the normalized frequency. Hence, the three-rows of air holes provide effective coupling and high isolation of the two bands. The optimal coupling length is 9.24 µm, very close to the value in the single-row case. The coupling length is 22 times the lattice constant. The insertion loss is slightly higher at the wavelength of 1.3 µm because of the increment in the number of separated rows, but the isolation ratio is increased considerably. Accordingly, the Demux with low insertion loss and an isolation of 24.2 and 27 dB can be obtained at wavelengths of 1.3 and 1.55 µm, respectively.

4 Bandwidth performance

As stated above, the aim is to design the DEMUX to have at least one wavelength band with a large bandwidth. The spectral responses of the PhC-based devices are analyzed using the FDTD method. Figure 9 plots the variation in the wavelength of a rod-based device. The insertion loss is relatively small and the bandwidth of the 1.3 µm wavelength band for >25 dB isolation exceeds 100 nm. In the 1.55 µm band, as presented in Fig. 9b, isolation >13 dB and

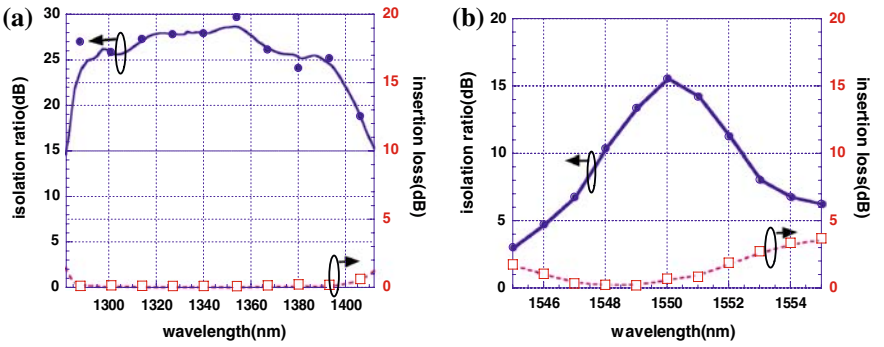

Fig. 9 Variation of insertion loss and isolation ratio with wavelength for the rod-based DBWD in the (**a**) 1.3 µm and (**b**) 1.55 µm wavelength band

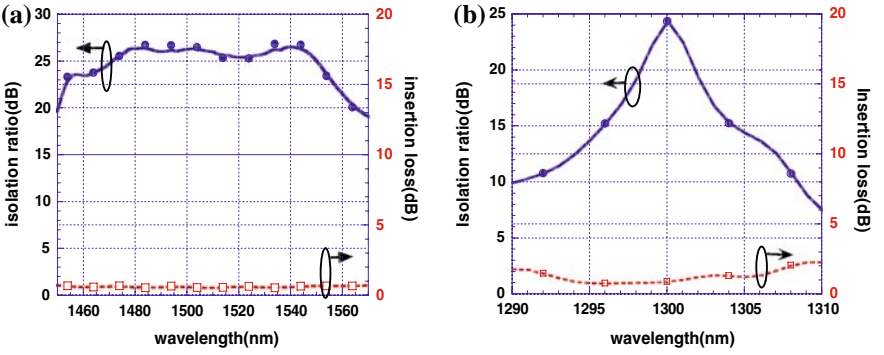

Fig. 10 Variation of insertion loss and isolation ratio with wavelength for the air-hole-based DBWD in the (**a**) 1.55 µm and (**b**) 1.3 µm wavelength band

a wavelength tolerance of around 5 nm is achieved. The circle and square symbols represent the isolation ratio and the insertion loss, respectively. Figure 10 plots the results concerning the hole-based DEMUX. The bandwidth of the 1.55 μm band for >25 dB isolation exceeds 100 nm. In the 1.3 μm band, as plotted in Fig. 10b, the device achieves >18 dB isolation with a wavelength tolerance of approximately 5 nm.

5 Conclusion

This paper depicts a novel design for PhC-based DEMUXs. The structure of the silicon material passes light of wavelengths of 1.3/1.55 μm by coupling and the PBG of PCs. The modes almost overlap in part of the range of PBG, which could result in the formation of a broadened bar state band. Based on the ideal 2D assumption, the FDTD simulation indicates that the two DEMUXs have a low insertion loss and a high isolation ratio. They have isolations of 25 and 16.8 dB, and 24.2 and 27 dB, at wavelengths of 1.3 and 1.55 μm, respectively. Although problems remain with the height of the PC slab, which may change the range of PBG, they can be eliminated by varying the radius of the holes and the effective index (Chung and Lee 2006). However, a realistic device will require further improvements.

Acknowledgements The authors would like to thank the Ministry of Economic Affairs of the Republic of China for financially supporting this research under Contract No. PSOC-91-EC-17-A-07-S1-0011.

References

Bayindir, M., Temelkuran, B., Ozbay, E.: Tight-binding description of the coupled defect modes in the three-dimensional photonic crystals. Phys. Rev. Lett. **84**, 2140–2143 (2000)

Boscolo, S., Midrio, M., Someda, C.G.: Coupling and decoupling of electromagnetic waves in parallel 2D photonic crystal waveguide. IEEE J. Quantum Electron. **38**, 47–53 (2002)

Chien, F.S.-S., Hsu, Y.J., Hsieh, W.-F., Cheng, S.-C.: Dual wavelength demultiplexng by coupling and decoupling of photonic crystal waveguides. Optics Express **12**, 1119 (2004)

Chung, L.W., Lee, S.L.: Multimode-interference-based broad-band demultiplexers with internal photonic crystals. Optics Express **14**, 4923–4927 (2006)

Chutinan, A., Okano, M., Noda, S.: Wider bandwidth with high transmission through waveguide bends in two-dimensional photonic crystal slabs. Appl. Phys. Lett. **80**, 1698–1700 (2002)

Costa, R., Melloni, A., Martinelli, M.: Experimental demonstration of photonic crystal directional coupler at microwave frequencies. Photon. Tech. Lett. **15**, 401 (2003)

Imelda, M., Noda, S., Chutinan, A., Mochizuki, M., Tanaka, T.J.: Channel drop filter using a single defect in a 2-D photonic crystal slab waveguide. Lightwave Tech. **20**, 873–878 (2002)

Johnson, S.G., Joannopoulos, J.D.: Optics Express **8**, 173 (2001)

Koshiba, M.: Wavelength division multiplexing and demultiplexing with photonic crystal waveguide couplers. J. Lightwave Tech. **19**, 1970–1975 (2001)

Martinez, A., Cuesta, F., Marti, J.: Ultrashort 2-D photonic crystal directional couplers. Photon. Tech. Lett. **15**, 694–696 (2003)

McNab, S., Moll, N., Vlasov, Y.: Ultra-low loss photonic integrated circuit with membrane-type photonic crystal waveguides. Optics Express **11**, 2927–2939 (2003)

Sharkawy, A., Shi, S., Prather, D.W.: Electro-optical switching using coupled photonic crystal waveguides. Optics Express **10**, 1048–1059 (2002)

Tanabe, T., Notomi, M., Kuramochi, E., Taniyama, H.: Large pulse delay and small group velocity achieved using ultrahigh-Q photonic crystal nanocavities. Optics Express **15**, 7826–7839 (2007)

Vlasov, Y., McNab, S.: Losses in single-mode silicon-on-insulator strip waveguides and bends. Optics Express **12**, 1622–1631 (2004)

Yablonovitch, E.: Inhibited spontaneous emission in solid–state physics and electronics. Phys. Rev. Lett. **58**, 2059–2062 (1987)